








Spectrally pure far-UVC emission from AlGaIn-based LEDs with dielectric band pass filters

Martin Guttman^{1,2,*} , Neysha Lobo-Ploch² , Heiko Gundlach³, Frank Mehnke¹ , Luca Sulmoni¹ , Tim Wernicke¹ , Hyun Kyong Cho² , Katrin Hilbrich², Alexander Külberg², Matthias Friedler², Thomas Filler², Indira K pplinger⁴, Dennis Mitrenga⁴, Christian Maier⁴, Olaf Brodersen⁴, Thomas Ortlepp⁴, Ulrike Woggon³, Sven Einfeldt²  and Michael Kneissl^{1,2} 

¹ Institute of Solid State Physics, Technische Universit t Berlin, Hardenbergstra e 36, 10623 Berlin, Germany

² Ferdinand-Braun-Institut gGmbH, Leibniz-Institut f r H chstfrequenztechnik, Gustav-Kirchhoff-Str. 4, 12489 Berlin, Germany

³ Institute of Optics and Atomic Physics, Technische Universit t Berlin, Stra e des 17. Juni 135, 10623 Berlin, Germany

⁴ CiS Forschungsinstitut f r Mikrosensorik GmbH, Konrad-Zuse-Str. 14, 99099 Erfurt, Germany

E-mail: martin.guttman@physik.tu-berlin.de

Received 15 December 2021, revised 20 January 2022

Accepted for publication 2 February 2022

Published 18 February 2022



Abstract

AlGaIn-based far ultraviolet-C (UVC) light emitting diodes (LEDs) with a peak emission wavelength below 240 nm typically show a long-wavelength tail at >240 nm that is detrimental to the use of the devices for skin-friendly antiseptics. We present the development of far-UVC LEDs with reduced long-wavelength emission using a HfO₂/SiO₂-based distributed Bragg reflector (DBR) filter. When the DBR filter is directly mounted on an LED package, the long-wavelength emission around 250 nm is reduced by two orders of magnitude while the transmitted output power is reduced down to 18%–27% of the initial value for DBR filters with cut-off wavelengths at 237–243 nm. As the transmission through the DBR filter depends strongly on the angle of incidence of the radiation, the transmitted output power of the spectrally pure far-UVC radiation can be doubled when an additional collimating lens is used on top of the LED package before passing through the filter.

Keywords: far-UVC, LED, AlGaIn, spectral purity, dielectric filter, HfO₂/SiO₂

(Some figures may appear in colour only in the online journal)

* Author to whom any correspondence should be addressed.



Original content from this work may be used under the terms of the [Creative Commons Attribution 4.0 licence](https://creativecommons.org/licenses/by/4.0/). Any further distribution of this work must maintain attribution to the author(s) and the title of the work, journal citation and DOI.

1. Introduction

AlGaIn-based ultraviolet-C (UVC) light emitting diodes (LEDs) have generated a large amount of interest in recent years since they offer a number of advantages over conventional ultraviolet light sources. UVC LEDs provide single peak emission and their emission wavelength can be easily tuned to fit the application, their operation voltages are low, they can be rapidly turned on and off, they are compact, and short pulsed operation is feasible [1–3]. UVC LEDs with an emission wavelength below 240 nm, hereafter referred to as far-UVC LEDs, are particularly interesting for applications such as monitoring of gas concentrations like NO or NH₃ [4, 5], measurement of nitrates in water [6], and antiseptics without mammalian skin damage [7–9]. However, the efficiency and output power of today's far-UVC LEDs are relatively low and decrease rapidly towards shorter wavelengths [10–15]. In addition, the spectral width of the far-UVC LED emission is typically in the range of 10–12 nm with stronger broadening on the long-wavelength side of the peak due to AlGaIn compositional fluctuations and quantum well thickness variations as well as changes in the polarization of the emitted light [16, 17].

For disinfection, UVC radiation <280 nm is very effective [18], due to its damage to the deoxyribonucleic acid (DNA) within viruses and bacteria. Consequently, this radiation is also able to damage the DNA within human skin cells. Recently it was demonstrated that excimer lamp radiation at 207 nm [7] and at 222 nm [8] as well as far-UVC LEDs with emission around 233 nm [9] can be used for the inactivation of multiresistant pathogens with negligible damage to the human skin. Nevertheless, spectral filters are required in order to reduce the skin-damaging long-wavelength UVC emission contribution.

In this paper, we present the development of spectrally pure far-UVC LEDs with reduced long-wavelength emission using a distributed Bragg reflector (DBR) filter integrated into the LED package. We show quantitatively the strong reduction in LED output power due to the angle dependent shift of the stop-band wavelength of the DBR filter combined with the nearly Lambertian-type far-field emission of the far-UVC LED. We will compare this approach to far-UVC LEDs with integrated optical lenses in combination with an external DBR filter on top of the irradiation module. The key challenge hereby is to maximize the suppression of unwanted long-wavelength UVC emission from the far-UVC LEDs while maximizing the remaining useful emission power in the far-UVC. A central question in this investigation is the angle dependent transmission through the filter and the corresponding shift of the DBR stop-band and its effects on the emission spectrum and on the far-field distribution of far-UVC LEDs.

2. Experimental

The far-UVC LED heterostructure was grown by metal organic vapor phase epitaxy on (0001) oriented epitaxially laterally overgrown (ELO) AlN/sapphire templates with 0.1° off-cut [19] with threading dislocation densities of

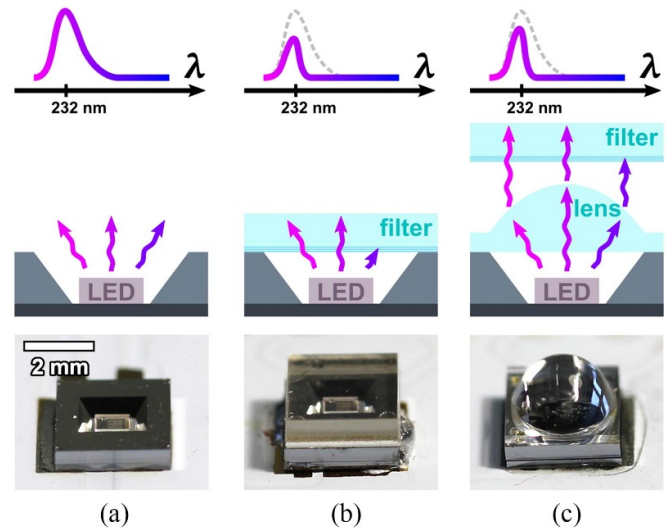


Figure 1. Schematic diagrams of the influence of the filter on the emitted spectrum (wavelength λ) and optical images of the flip-chip mounted LED in the package with an integrated aluminum reflector (a) without a filter, (b) with a DBR filter lid, and (c) with a plano-convex quartz glass lens and an additional DBR filter plate.

$1.4 \times 10^9 \text{ cm}^{-2}$ [20]. The heterostructure consists of a 1.2 μm thick Al_{0.87}Ga_{0.13}N:Si current spreading layer, a three-fold multiple quantum well active region with 1 nm thick Al_{0.72}Ga_{0.28}N quantum wells and 5 nm thick Al_{0.83}Ga_{0.17}N:Si delta-doped barriers, a 6 nm thick AlN electron blocking layer, and an UV-absorbing p-side with Al_{0.8}Ga_{0.2}N:Mg/Al_{0.7}Ga_{0.3}N:Mg and Al_{0.37}Ga_{0.63}N:Mg/Al_{0.2}Ga_{0.8}N:Mg short period superlattices and a 40 nm thick GaN:Mg contact layer [13]. The wafers were processed with standard micro-fabrication techniques to LEDs with an actively emitting area of 0.157 mm² and 0.485 mm² using Pt-based p-contacts and V/Al-based n-contacts [21]. After dicing, 1.06 mm \times 0.66 mm and 1 mm \times 1 mm chips were flip-chip mounted on Si-based surface-mounted device (SMD) packages with an integrated aluminum reflector [22] as shown in figure 1(a).

All DBR filters consist of a HfO₂/SiO₂ multilayer stack deposited using a Böhler ‘Syrus 710 pro’ deposition system with two electron beam guns (EBG) and ion support (‘APS pro’). The layer thickness was measured during the coating using a reference quartz crystal. The filter has a short-pass design with a layer sequence (HL)¹⁷ H 0.5 L (H: 31.8 nm HfO₂, L: 43.7 nm SiO₂) which was optimized by simulations using the transfer-matrix method. In order to minimize the reflections in the range of the desired emission wavelength and achieving a high slope of the stop-band edge, the individual layer thicknesses were varied iteratively by a random method. The edge wavelength could be adjusted by changing L and H by the same factor. In practice this happens, e.g. when the position of the substrates in the coating chamber is changed. The design was optimized for the deposition on 1 mm thick and 10 cm \times 10 cm far-UVC-transparent quartz substrates, which are used in combination with packaged LEDs including a plano-convex quartz glass lens from NGK *insulators, ltd* (module-level approach, figure 1(c)). This lens has

a parabolic shape with a total height of 1.8 mm and a base diameter of 3.2 mm. Together with the quartz substrates, 1 mm thick and 1''-diameter sapphire substrates were also coated. As a result of different positions of these substrates in the chamber and manufacturing tolerances the transmission spectra of the individual filters on sapphire differ. Three filters on sapphire substrates whose transmittance matched the LED emission wavelength of 232 nm were selected, diced into 3.5 mm × 3.5 mm square-shaped lids and mounted on the packages (chip-level approach, figure 1(b)).

For transmission measurements, a *Shimadzu* 'UV-2600' UV-VIS spectrophotometer was used in free beam configuration orthogonal to the surface. The angle dependent emission spectra and radiant intensity of the LEDs were measured at room temperature at a constant current of 40 mA by a two axes rotation stage using a radiometric and wavelength calibrated *StellarNet* 'EPP2000' UV-VIS compact spectrophotometer and a calibrated UV-enhanced Si-photodiode with an active area of 0.8 mm² at a distance of 37 mm from the LED. For the far-UVC LED irradiation module, the irradiance was measured at room temperature at a constant current of 170 mA by a radiometrically calibrated photodetector ('UV-Surface-USB' by *sglux GmbH*) which was attached to a motorized xyz-stage to scan the radiation pattern at different positions and distances.

3. Results and discussion

3.1. Spectral properties of the filter and the LED emission

Figure 2 shows the transmission spectra of three different DBR filters under normal incidence as well as a typical normalized LED emission spectrum as a reference. All DBR filters show oscillations above 300 nm from high order interference effects, a broad stop-band between 240 nm and 300 nm, a transmission channel around the LED emission wavelength of 232 nm, and an absorption tail below 225 nm due to the increasing absorption coefficient of HfO₂ [23]. The position of the short-wavelength band edge of the stop-band, i.e. the cut-off wavelength, is defined as wavelength where a transmission of 50% of the maximum transmission around 235 nm is reached. These values are 237.4 nm for filter S (short), 240.1 nm for filter M (middle), and 242.7 nm for filter L (long). Due to the shift of the cut-off wavelength to shorter wavelengths with increasing angle of incidence [24], the performance of the filter strongly depends on the far-field distribution of the LED.

Figure 3 shows the emission spectra of two far-UVC LEDs measured before and after mounting a filter S lid (figure 3(a)) and a filter L lid (figure 3(b)) for polar emission angles between 0° (normal to the SMD plane) and 60°. Without a filter lid, both LEDs show an identical emission spectrum for all emission angles. With increasing polar emission angle, the peak position and shape of the spectra remain identical but the spectral intensity decreases, following the typical far-field radiation pattern of LEDs in a package with an integrated aluminum reflector [22]. When mounting either a filter S lid

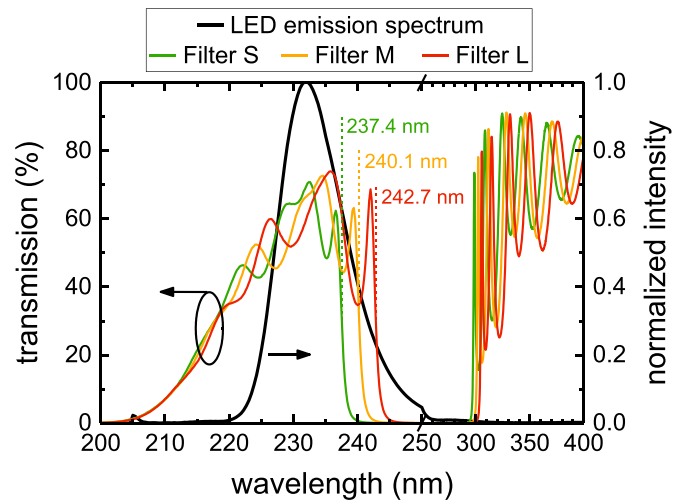


Figure 2. Normalized far-UVC LED emission spectrum (black) and transmission spectrum of three different DBR filters with a cut-off wavelength (50% of the local peak transmission) of 237.4 nm (green), 240.1 nm (yellow), and 242.7 nm (red) measured under normal incidence. Note the changed scale of the wavelength axis at 250 nm.

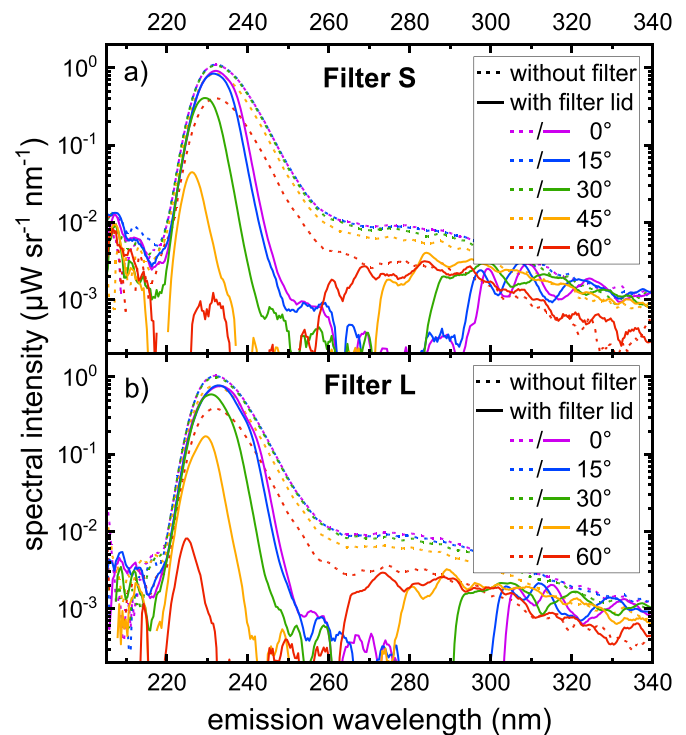


Figure 3. Angle dependent emission spectra of far-UVC LEDs without (dashed lines) and with (solid lines) a DBR filter lid with a cut-off wavelength of (a) 237.4 nm (Filter S) and (b) 242.7 nm (Filter L) for various polar emission angles between 0° (normal to the SMD plane) and 60°.

or a filter L lid on these LEDs, the spectra change substantially. The far-UVC emission peak becomes narrower due to the reduction of long-wavelength emission contributions by more than two orders of magnitude in the stop-band range of the DBR filter, e.g. at 250 nm. As the cut-off wavelength of the

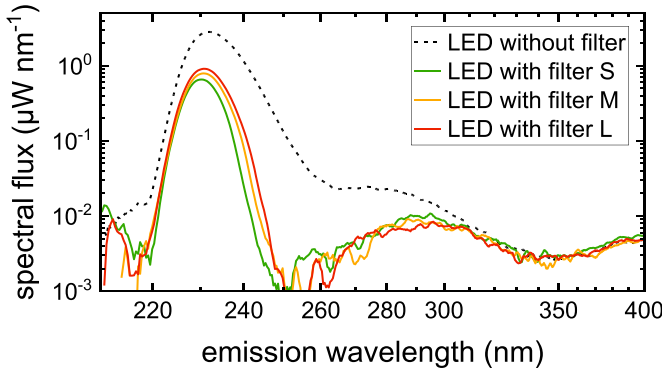


Figure 4. Total emission spectrum (integrated over all solid angles) of a far-UVC LED without filter lid (black dashed line) and of LEDs with a DBR filter lid S, M, and L (solid lines).

DBR filter decreases with increasing angle of incidence, also the peak emission wavelength shifts from 232 nm (without filter) to shorter wavelengths, e.g. to 226 nm for filter S and to 229.5 for filter L at 45° . Consequently, the integrated intensity reduces significantly with increasing emission angle. On the other hand, the long-wavelength edge of the DBR filter stop-band shifts for angles between 0° and 60° by roughly 40 nm from 305 nm to 265 nm for filter L and from 295 nm to 255 nm for filter S. The latter can result in partial transmission of long-wavelength emission at high polar angles. This effect must be suppressed by an LED package design that results in directional radiation, in order to avoid unwanted long-wavelength emission from the LED despite a filter.

Figure 4 shows the total emission spectra, i.e. the emission integrated over all solid angles, of an LED without a filter and of LEDs with an additional lid using filter S, M, and L. Without a filter, the LED emission peaks at 232 nm with a full width at half maximum (FWHM) of 12 nm. The corresponding full width at 1% of the maximum is close to 40 nm and the peak has a tail on the long-wavelength side. With a filter lid, the peak emission wavelength is slightly shortened to 230–231 nm and the spectral flux of wavelengths around 250 nm is reduced by two orders of magnitude. The suppression of the long-wavelength emission tail near 250 nm leads to a reduction in the FWHM to 9.9 nm and to 8.8 nm while the full width at 1% of the maximum is reduced even more to 26 nm and to 20 nm in the case of filter L and S, respectively. However, the optimal filter is not only characterized by its spectral purity but also by the remaining useful power output.

3.2. Far-field distribution and total output power

Figure 5(a) shows the measured far-field emission distribution of far-UVC LEDs without a filter lid as well as the identical LEDs with an additional lid using the filter S, M, and L, respectively. The package with an integrated aluminum reflector results in a relatively broad far-field with a viewing angle (FWHM) of 110° and emission at polar angles of up to $\pm 75^\circ$. Mounting the filter lid on top of the package strongly narrows the far-field for all filters. In particular, the viewing

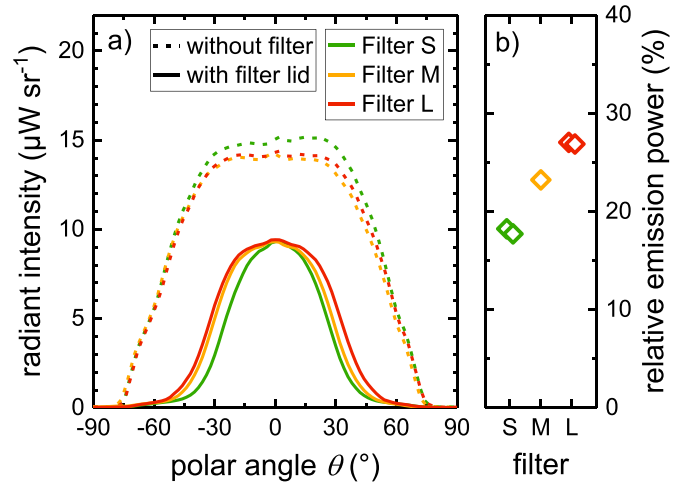


Figure 5. (a) Far-field emission distribution of far-UVC LEDs in the package without filter lid (dashed line) and with a DBR filter lid (solid line) with filter S (green), M (yellow), and L (red). (b) Transmitted output power of the far-UVC LEDs with additional DBR filter lid relative to the emission power of the LED without filter in case of filter S, M, and L.

angle is reduced to 65° in case of the LED with filter L and to 50° in case of the LED with filter S. This narrowing is a direct consequence of the shift in the cut-off wavelength of the filter with increasing polar emission angle as discussed previously. Furthermore, even at 0° the radiant intensity is reduced to 70% of its initial value due to the limited transparency of the investigated filter at the peak emission wavelength of the far-UVC LED. Both effects strongly reduce the total emission power for these devices. In particular, the total emission output power with the filter is 18%, 23%, and 27% of the value without the filter in the case of LEDs with the filter S, M, and L, respectively, as shown in figure 5(b). As the difference in integral transmission of filter S, M, and L is significant in spite of small changes in the spectral properties, an investigation of the biological effects of different spectra is necessary to fix the optimal cut-off wavelength of the filter.

As a large portion of the light emitted at higher angles is blocked by the filter, one approach to enhance light transmission through the filter is to collimate the LED emission before passing the filter. Therefore, ray-tracing simulations for different LED packages including an additional lens were performed (published elsewhere) considering the spatial and spectral radiation pattern of the LED chip [25], the geometry of the lens, and the angle dependent transmission through filter M. Figure 6 shows the simulated effective light extraction efficiency (LEE) from the LED chip as a function of the detector viewing angle for different packaging concepts: (I) an open package (compare figure 1(a)), (II) a package with a DBR filter in front, (III) a package with a lens, and (IV) a package with a lens and a DBR filter in front (compare figure 1(c)). In case of an open package (case I), the simulated effective LEE increases with increasing viewing angle due to the broad far-field distribution of the emission and due to the increasing solid angle range covered. When adding a DBR filter in front

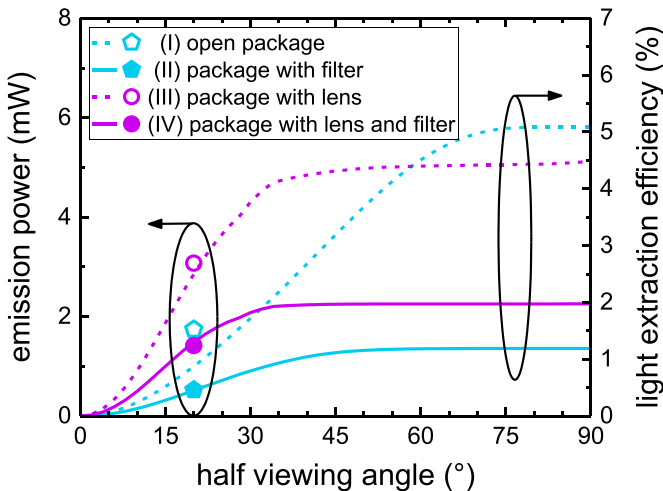


Figure 6. Simulated effective light extraction efficiency (solid lines) as a function of the detector viewing angle and measured emission power of the module (single data points) within a half viewing angle of 20° for an open package, a package with a filter lid, a package with a lens, and a package with a lens and a filter.

(case II), the simulated effective LEE for large half viewing angles ($>75^\circ$) is reduced by more than a factor of four from 5.1% to 1.2% consistent with the results in figure 5(b). Light which is emitted to angles larger than 45° cannot pass through the filter as it can be seen in the constant LEE for half viewing angles $>45^\circ$. By adding a lens to the package (case III), the effective LEE increases stronger along the viewing angle due to the more collimated emission. Especially for half viewing angles below 35° , the LEE increases by nearly a factor of two. For large viewing angles, the effective LEE is 4.5% rather than 5.1% as for the open package due to reflection losses at the lens surfaces. When the transmission through the DBR filter is included (case IV), the simulated effective LEE for large viewing angles decreases from 4.5% to 2%. However, this is still a factor of almost two higher than in case of the package with the filter lid but without lens (case II).

To verify the simulation results, irradiation modules with arrays of four LEDs packaged either with or without additional lens were measured with and without the DBR filter plate in front. Here, the photodetector was placed 5 cm below the module frame (10 cm below the LEDs) leading to a detector half viewing angle of 20° . Figure 6 shows the measured emission power of the module as single data points at 20° . The ratios of the emission powers for the various packaging concepts are in good agreement with the predicted values from the simulation at this viewing angle. Here, the gain of emission power behind the filter is $\sim 170\%$ when using a package with lens (1.4 mW, case IV) instead of an open package without lens (0.5 mW, case II). The difference between simulation and measurement in case of the open package without a filter (case I) can be attributed to the Al-coated module frame [9], reflecting the light which is emitted into the solid angle between 45° and 55° . For LEDs with a lens and/or the filter plate, the contribution of such reflected light can be neglected.

The results show the importance of considering the angle dependent DBR filter transmission and the far-field

distribution of LEDs when designing a spectrally pure far-UVC irradiation module with LEDs. In particular, a collimated LED emission is advantageous to achieve an efficient transmission through a dielectric spectral filter. Similar to Glaab *et al* [9], a module was equipped with a total of 120 LEDs, each with a peak emission wavelength of 233 nm and an output power of 1 mW at a current of 170 mA. The LEDs each equipped with a lens and a filter plate in front as described above were operated at a current of 170 mA at a heat sink temperature of 18°C leading to a spectrally pure emission with low spectral contributions for wavelengths $>240\text{ nm}$. The irradiance measured 5 cm below the module is 0.37 mW cm^{-2} , uniform within an area of 7 cm in diameter. This is a factor of eight higher than previously reported [9] enabling a more efficient disinfection.

4. Summary

In summary, we have studied different concepts for a spectrally pure far-UVC irradiation system based on AlGaIn-based far-UVC LEDs. The LEDs had a peak emission wavelength of 232 nm with a long-wavelength UVC tail which was suppressed by a $\text{HfO}_2/\text{SiO}_2$ -based DBR filter with as little reduction in far-UVC output as possible. The filter was either integrated in the LED package (chip-level approach) or placed outside the package using an additional lens (module-level approach). DBR filters with cut-off wavelengths at 237–243 nm integrated into the LED package reduce the long-wavelength emission around 250 nm by two orders of magnitude, but at the same time transmit only 18%–27% of the total output power of the LED. Here, the cut-off wavelength has a strong impact on the integral transmission but a small impact on the spectral purity of the LEDs. Due to the broad LED far-field distribution in combination with the angle dependence of the cut-off wavelength of the DBR filter, the light transmission through the filter was enhanced by using a collimating lens in the LED package. As predicted by ray-tracing simulations and confirmed by measurements, the output power that can be used after the filter was increased by 170% within a half viewing angle of 20° and nearly doubled for even larger viewing angles using LEDs with a plano-convex lens in comparison to LEDs without a lens.

Data availability statement

The data that support the findings of this study are available upon reasonable request from the authors.

Acknowledgments

The authors would like to thank Sylvia Hagedorn (Ferdinand-Braun-Institut gGmbH, Leibniz-Institut für Höchstfrequenztechnik, Berlin, Germany) for providing the ELO AlN/sapphire templates for the LEDs. This work was partially supported by the German Federal Ministry of Education and Research (BMBF) within the ‘Advanced UV for

life—VIMRE’ and ‘CORSA’ projects under the contracts 03ZZ0146C, 03ZZ0146D, and 03COV10D.

ORCID iDs

Martin Guttman  <https://orcid.org/0000-0002-4697-3145>

Neysha Lobo-Ploch  <https://orcid.org/0000-0002-3901-1423>

Frank Mehnke  <https://orcid.org/0000-0001-5406-0832>

Luca Sulmoni  <https://orcid.org/0000-0002-5341-7032>

Tim Wernicke  <https://orcid.org/0000-0002-5472-8166>

Hyun Kyong Cho  <https://orcid.org/0000-0001-5540-2582>

Sven Einfeldt  <https://orcid.org/0000-0001-7502-7812>

Michael Kneissl  <https://orcid.org/0000-0003-1476-598X>

References

- [1] Muramoto Y, Kimura M and Nouda S 2014 *Semicond. Sci. Technol.* **29** 084004
- [2] Kneissl M, Seong T Y, Han J and Amano H 2019 *Nat. Photon.* **13** 233
- [3] Amano H *et al* 2020 *J. Appl. Phys.* **53** 503001
- [4] Mellqvist J, Axelsson H and Rosén A 1996 *J. Quant. Spectrosc. Radiat. Transfer* **56** 225–40
- [5] Mehnke F *et al* 2017 *IEEE J. Sel. Top. Quantum Electron.* **23** 29
- [6] Thomas O, Gallot S and Mazas N 1990 *Fresenius J. Anal. Chem.* **338** 238–40
- [7] Buonanno M, Stanislauskas M, Ponnaiya B, Bigelow A W, Randers-Pehrson G, Xu Y, Shuryak I, Smilenov L, Owens D M and Brenner D J 2016 *PLoS One* **11** e0138418
- [8] Buonanno M, Ponnaiya B, Welch D, Stanislauskas M, Randers-Pehrson G, Smilenov L, Lowy F D, Owens D M and Brenner D J 2017 *Radiat. Res.* **187** 493
- [9] Glaab J *et al* 2021 *Sci. Rep.* **11** 14647
- [10] Hirayama H, Fujikawa S, Noguchi N, Norimatsu J, Takano T, Tsubaki K and Kamata N 2009 *Phys. Status Solidi a* **206** 1176–82
- [11] Moe C G, Sugiyama S, Kasai J, Gradusky R and Schowalter L J 2017 *Phys. Status Solidi a* **215** 1700660
- [12] Liu D *et al* 2018 *Appl. Phys. Lett.* **113** 011111
- [13] Mehnke F, Sulmoni L, Guttman M, Wernicke T and Kneissl M 2019 *Appl. Phys. Express* **12** 012008
- [14] Yoshikawa A, Hasegawa R, Morishita T, Nagase K, Yamada S, Grandusky J, Mann J, Miller A and Schowalter L J 2020 *Appl. Phys. Express* **13** 022001
- [15] Lobo-Ploch N, Mehnke F, Sulmoni L, Cho H K, Guttman M, Glaab J, Hilbrich K, Wernicke T, Einfeldt S and Kneissl M 2020 *Appl. Phys. Lett.* **117** 111102
- [16] Römer F, Guttman M, Wernicke T, Kneissl M and Witzigmann B 2021 *Materials* **14** 7890
- [17] Guttman M, Mehnke F, Belde B, Wolf F, Reich C, Sulmoni L, Wernicke T and Kneissl M 2019 *Jpn. J. Appl. Phys.* **58** SCCB20
- [18] Mamane-Gravetz H, Linden K G, Cabaj A and Sommer R 2005 *Environ. Sci. Technol.* **39** 7845–52
- [19] Enslin J, Knauer A, Mogilatenko A, Mehnke F, Martens M, Kuhn C, Wernicke T, Weyers M and Kneissl M 2019 *Phys. Status Solidi a* **216** 1900682
- [20] Susilo N *et al* 2020 *Photon. Res.* **8** 589–94
- [21] Sulmoni L, Mehnke F, Mogilatenko A, Guttman M, Wernicke T and Kneissl M 2020 *Photon. Res.* **8** 1381–7
- [22] Kaepplinger I, Taeschner R, Mitrenga D, Karolewski D, Li L, Meier C, Schaedel M and Ortlepp T 2019 *Proc. SPIE* **10940** 35–45
- [23] Khoshman J M and Kordesch M E 2006 *Surf. Coat. Technol.* **201** 3530–5
- [24] Zhou S, Xu H, Liu M, Liu X, Zhao J, Li N and Liu S 2018 *Micromachines* **9** 650
- [25] Guttman M 2020 *PhD Thesis* Technische Universität Berlin DepositOnce 10590